RSC Advances

PAPER

View Article Online
View Journal | View Issue

Cite this: *RSC Adv.*, 2024, **14**, 18970

Enhanced fluorometric detection of histamine using red emissive amino acid-functionalized bimetallic nanoclusters†

Yahya S. Alqahtani,[a] Ashraf M. Mahmoud,[a] Al-Montaser Bellah H. Ali[b] and Mohamed M. El-Wekil *[b]

Received 18th March 2024
Accepted 3rd June 2024

DOI: 10.1039/d4ra02010c

rsc.li/rsc-advances

Lysine-capped gold nanoclusters doped with silver (LYS@Ag/Au NCs) have been developed for the sensitive and selective "turn-off" fluorescence detection of histamine. This fluorescent probe demonstrates excellent stability and a high quantum yield of 9.45%. Upon addition of histamine, a positively charged biogenic amine, to the LYS@Ag/Au NCs fluorescent probe, its fluorescence emission is quenched due to electrostatic interaction, aggregation, and hydrogen bond formation. The probe exhibits good sensitivity for the determination of histamine within the range of 0.003–350 μM, with a detection limit of 0.001 μM based on a signal-to-noise ratio of 3. Furthermore, the probe has been applied to detect biogenic amines in complicated matrices, highlighting its potential for practical applications. However, interference from the analogue histidine was observed during analysis, which can be mitigated by using a Supelclean™ LC-SAX solid-phase extraction column for removal.

1. Introduction

The safety and quality of food have become increasingly prominent concerns worldwide. Improper storage practices can lead to the formation of various harmful compounds, among which histamine stands out.[1] Histamine is recognized as a significant biomarker for food spoilage. Ingesting certain concentrations of histamine can result in adverse effects, including diarrhea, urticaria, headache, and abdominal pain.[2] Regulatory bodies have established maximum limits for histamine levels in fish, set at 0.2 g kg^{-1} for fresh fish and 0.4 g kg^{-1} for cured fish products.[3] It is worth noting that histamine is not confined to fish; other food items such as cheese, meat, and fermented beverages can also contain histamine.[4] The Food and Drug Administration (FDA) and the European Union (EU) enforce more stringent regulations, with limits set at 50 mg kg^{-1}[5] and 100 mg kg^{-1},[6] respectively. The lack of a chromophore moiety in histamine poses a challenge for its measurement, whether through UV/vis spectroscopy or direct fluorometric technique.[7] Optically measuring histamine requires derivatization with orthophthaldhyde, which introduces non-selectivity due to its reaction with other amino acids.[8] Consequently, this derivatization method may not accurately quantify histamine levels, as it can lead to interference from other compounds containing amino groups. Additional analytical methods used for the determination of histamine include GC/MS,[9] TLC,[10] HPLC,[11] and ELISA.[12] However, these methods often come with drawbacks. They are expensive due to the equipment and reagents required, involve extensive pretreatment steps, demand skilled personnel for operation, and are time-consuming.[13–15] These factors may limit their practicality and accessibility, especially in settings where resources are limited or rapid analysis is essential. Fluorescence detection methods have garnered significant attention due to their simplicity, rapidity, satisfactory selectivity, cost-effectiveness, and high sensitivity.[16,17] These methods offer several advantages over other analytical techniques, making them increasingly popular for a wide range of applications. Numerous studies have explored the fluorometric detection of histamine using various advanced materials such as carbon nitride,[18] quantum dots,[19] metal–organic frameworks,[20] and upconversion nanoparticles.[21] Indeed, metal nanoclusters have garnered significant interest.[22] Their diminutive scale and distinctive characteristics render them particularly intriguing for a multitude of applications.[23] These nanoclusters demonstrate intriguing chemical, physical, and optical properties, stemming from quantum confinement effects and surface properties.[24] Consequently, they find applications across diverse fields including catalysis, electronics, sensing, and biomedicine. Their unique attributes make them promising candidates for enhancing the sensitivity and selectivity of analytical techniques, such as in the fluorometric detection of histamine. Indeed, bimetallic nanoclusters have been found to

[a]*Department of Pharmaceutical Chemistry, College of Pharmacy, Najran University, Najran 11001, Saudi Arabia. E-mail: mohamed.mohamoud@ymail.com*

[b]*Department of Pharmaceutical Analytical Chemistry, Faculty of Pharmacy, Assiut University, Assiut 71516, Egypt. E-mail: mohamed.elwakeel@pharm.aun.edu.eg*

† Electronic supplementary information (ESI) available. See DOI: https://doi.org/10.1039/d4ra02010c

exhibit greater stability and higher photoluminescence quantum yields compared to their monometallic counterparts.[25] This enhancement in properties arises from synergistic interactions between the two different metals, leading to improved electronic structure and optical properties. For example, in the case of gold (Au) nanoclusters, the incorporation of silver (Ag) atoms has been shown to enhance the photoluminescence quantum yield.[26] The introduction of Ag atoms can modify the electronic structure and surface properties of the Au nanoclusters, leading to improved emission efficiency. This synergistic effect between Au and Ag atoms demonstrates the potential of bimetallic nanoclusters for optimizing the performance of various applications, including sensing and fluorescence-based detection methods like those used for histamine detection. Lysine (LYS) is an essential amino acid characterized by its basic nature, featuring two amino groups and one carboxylic acid moiety. When incorporated into nanoparticle formulations, LYS plays a crucial role in stabilizing the particles within a solution through electrostatic interactions, enhancing their dispersibility in water.[27] Furthermore, its versatile chemical structure enables LYS to engage with various analytes through a range of interaction forces, including electrostatic interaction and non-covalent hydrogen bonding.

In this study, bimetallic nanoclusters (Ag/Au NCs) were stabilized using lysine amino acid (LYS@Ag/Au NCs) for the purpose of sensitively and selectively detecting histamine in human serum samples. The reaction of histamine and LYS@Ag/Au NCs resulted in the quenching of red emission at 640 nm, with quenching intensity increasing proportionally with the concentration of histamine. This interaction is attributed to various bonding mechanisms, including hydrogen bonding and hydrophobic interactions, underscoring the complexity of the histamine–NCs interaction and the potential for precise detection methods.

2. Experimental

2.1. Materials and reagents

Histamine (97.2%), lysine (98.4%), serotonin (97.7%), spermine (97.8%), epinephrine (97.4%), spermidine (98.4%), tryptamine (96.7%), tyramine (97.7%), histidine (97.3%), ascorbic acid (96.3%), dopamine (96.8%), cadaverine (97.7%), phenylalanine (98.3%), glutathione (98.3%), silver nitrate ($AgNO_3$), and tetrachloroauric acid trihydrate ($HAuCl_4 \cdot 3H_2O$) were procured from Sigma Aldrich. NaOH, HCl, sodium citrate, and HNO_3 were obtained from Merck.

2.2. Instrumentation, quantum yield LYS@Ag/Au NCs, and samples preparation

ESI† contains more details regarding instruments, quantum yield, and samples preparation.

2.3. Preparation of LYS@Ag/Au NCs

The glassware preparation involved soaking in HNO_3/HCl in a ratio of 1 : 3, v/v for approximately 30 minutes, followed by thorough washing with ultrapure water, repeating the process four times. To initiate the synthesis, 2.5 mL of a 0.015 M lysine solution was combined with 2.0 mL of $HAuCl_4 \cdot 3H_2O$ (2.0 mL, 24 mM) and $AgNO_3$ (2.0 mL, 6 mM) under stirring. After that

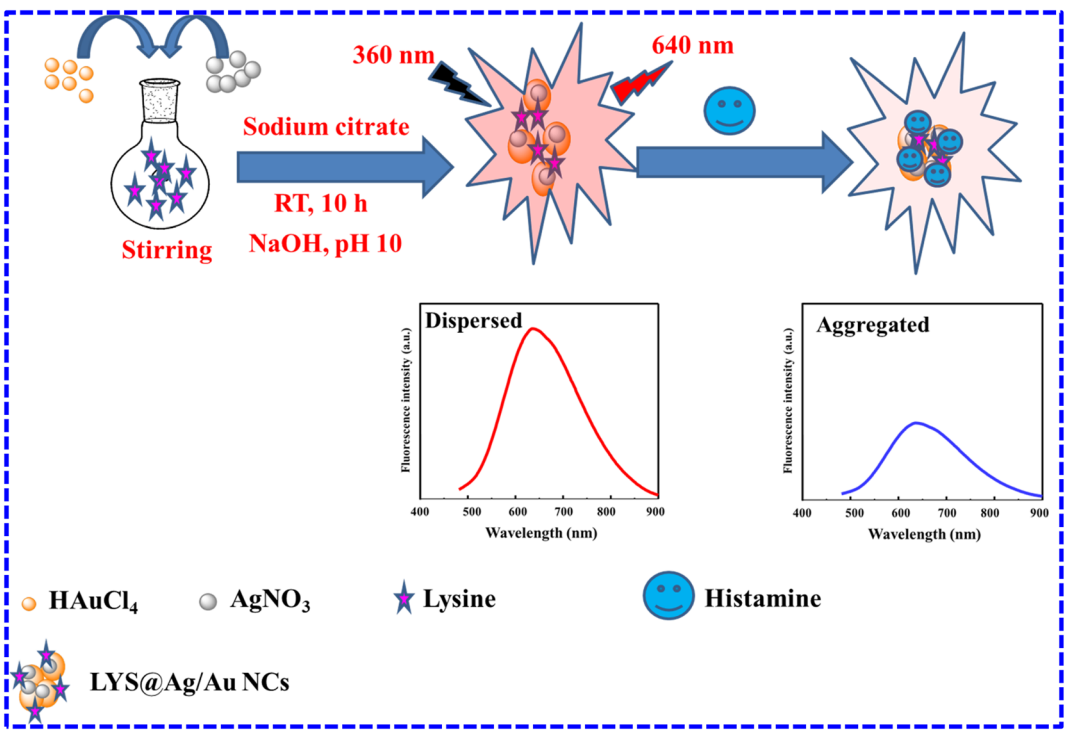

Scheme 1 Steps for preparation of LYS@Ag/Au NCs and fluorometric determination of histamine.

0.5 mL of 400 mM sodium citrate was added under stirring. The reaction was completed at room temperature (RT) for 10 hours. Subsequently, the volume was adjusted to 8.0 mL using ultrapure water. To achieve a pH of 10, NaOH solution (0.5 M) was added portionwise. The reaction was then carried out at 37 °C for an additional 10 hours at 1000 rpm. Finally, the resulting product was isolated through centrifugation at 3500 rpm for 25 minutes. The produced NCs were re-dispersed in 10 mL ultrapure water, followed by storage at 4 °C until further use. As controls, LYS@Ag NCs and LYS@Au NCs were prepared under the same conditions without addition of $HAuCl_4 \cdot 3H_2O$ and $AgNO_3$, respectively (Scheme 1).

2.4. Detection procedures

To perform the analysis, 300 μL of LYS@Ag/Au NCs was combined with varying quantities of histamine (450 μL) and incubated at RT for 3 minutes. Subsequently, the volume was adjusted to 1.0 mL using ultrapure water. Finally, the fluorescence responses were measured at 640 nm after excitation at 360 nm (Scheme 1).

3. Results and discussion

3.1. Characterization

The morphological characterization of the as-synthesized LYS@Au NCs and LYS@Ag/Au NCs was confirmed through TEM analysis. Fig. 1A and B display TEM images of LYS@Au NCs and LYS@Ag/Au NCs, respectively, revealing a well-dispersed and spherical pattern. The size distribution of particles in LYS@Au NCs and LYS@Ag/Au NCs is illustrated in Fig. 1C and D, respectively. It was observed that the average diameters of LYS@Au NCs and LYS@Ag/Au NCs are 2.7 nm ± 0.16 nm and 3.6 nm ± 0.21 nm, respectively. These results confirmed that the doping of silver (Ag) slightly increased the average diameter. High-resolution TEM (HRTEM) images (insets) further confirm the morphological details, showing lattice spacing value of 0.22 nm for LYS@Au NCs, which is corresponding to the *d*-spacing of the crystal plane of face centered cubic Au (111).[28] In addition, the lattice spacing for LYS@Ag/Au NCs was found to be 0.202 nm, which is corresponding to the *d*-spacing of the crystal plane of face centered cubic Au (111) and Ag (200).[29] Fig. 1E and F present the DLS patterns of LYS@Au NCs and LYS@Ag/Au NCs, respectively. The average diameters recorded are 13.79 ± 0.46 nm and 86.5 ± 4.34 nm, respectively. These measurements closely align with TEM analysis, providing further validation of the nanoparticle sizes. It is important to note that the particle sizes determined by DLS tend to be larger than those estimated by TEM. This difference could be attributed to the level of hydration and swelling experienced by these nanoparticles in water.[30,31]

Fig. S1A† explores the functionalization of Ag/Au NCs with lysine amino acid (LYS). In Fig. S1A(a),† the FTIR spectrum of LYS exhibits main absorption bands at 3358 cm^{-1}, 3305 cm^{-1}, 2808–2980 cm^{-1}, 1725 cm^{-1}, 1688 cm^{-1}, 1265 cm^{-1}, and 742 cm^{-1}, corresponding to ν (NH), ν (CH_2), ν (C=O), δ (OH, NH), δ (COO^-), and δ (NH) vibrations, respectively.[32,33] Interaction of LYS amino acid with Ag/Au NCs led to a shifting of the wavenumbers to lower values, indicating chemical interaction between them. The lack of the absorption band at 742 cm^{-1} in Fig. S1A(b)† confirms the chemical reaction between bimetallic nanoclusters and the amino acid, suggesting the modification of Ag/Au NCs with the amino acid.[34] Fig. S1B† presents the XRD pattern of LYS@ Ag/Au NCs with diffraction peaks at 31.8° and 46.3°, corresponding to face centered cubic Au (111) and Ag (200), respectively. Fig. S1C† illustrates the EDX pattern of the as-prepared LYS@Ag/Au NCs, revealing sharp peaks corresponding to C, O, N, Ag, and Au. These peaks indicate the

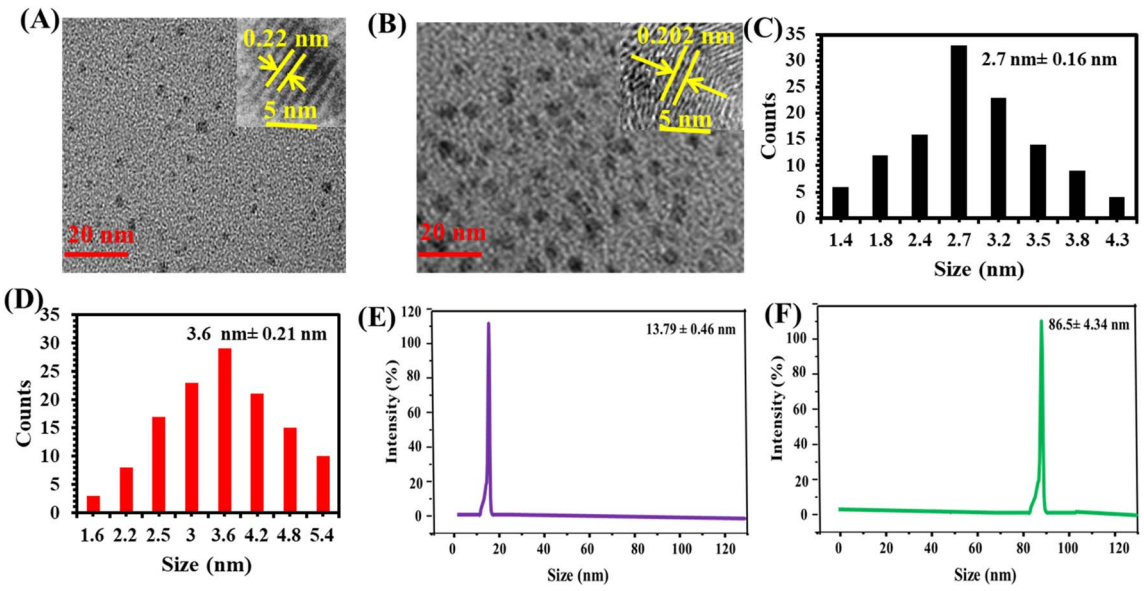

Fig. 1 TEM images of LYS@Au NCs (A) and LYS@Ag/Au NCs (B); size distribution of LYS@Au NCs (C) and LYS@Ag/Au NCs (D); DLS of LYS@Au NCs (E) and LYS@Ag/Au NCs (F).

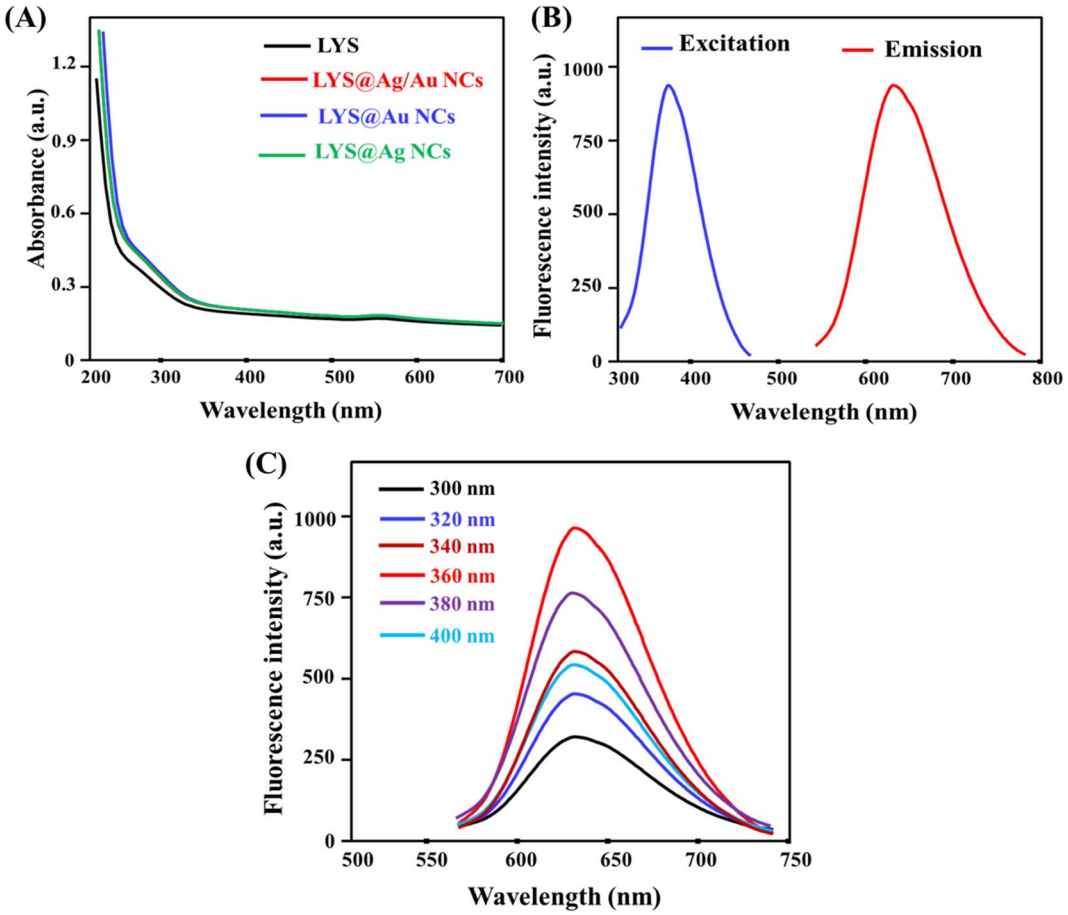

Fig. 2 (A) UV/visible spectra of LYS, LYS@Ag/Au NCs, LYS@Au NCs, and LYS@Ag NCs; (B) excitation and emission spectra of LYS@Ag/Au NCs; (C) emission behavior of LYS@Ag/Au NCs at various excitation wavelengths.

successful formation of LYS@Ag/Au NCs. The percentages of Ag and Au obtained by EDX are 1.66% and 6.64%, respectively, suggesting the molar ratio of Ag and Au is 1 : 4. Fig. S2A† presents the XPS pattern of the as-fabricated LYS@Ag/Au NCs, revealing distinctive peaks corresponding to C 1s, O 1s, N 1s, Ag 3d, and Au 4f. In Fig. S2B,† the high-resolution spectrum of Au 4f displays sharp peaks at 83.4 eV and 86.8 eV, corresponding to Au $4f_{7/2}$ and Au $4f_{5/2}$, respectively.[35] Fig. S2C† depicts the high-resolution spectrum of Ag 3d, exhibiting distinct peaks at 368.6 eV and 370.8 eV, assigned to Ag $3d_{5/2}$ and Ag $3d_{7/2}$, respectively.[35] The UV/visible spectrum of the as-prepared LYS@Ag/Au NCs was analyzed in Fig. 2A, revealing the lack of surface plasmon resonance observed for Ag and Au nanoparticles in this region indicating that the LYS@Ag/Au NCs were synthesized without presence of larger particles.[36] Moreover, the UV/visible spectra of LYS, LYS@Ag/Au NCs, LYS@Au NCs, and LYS@Ag NCs were recorded. It was found that they have nearly the same absorbance values, suggesting the presence of the same concentration of LYS on the surface of the NCs. Additionally; the fluorescence excitation spectra of LYS@Ag/Au NCs are located at 640 nm and 360 nm, respectively, as illustrated in Fig. 2B. Furthermore, it was concluded that the emission wavelengths remain consistent regardless of the excitation wavelengths, as shown in Fig. 2C. The stability of the LYS@Ag/Au NCs was further assessed under various conditions, including variations in ionic strength, pH, temperature, and irradiation time, as depicted in Fig. S3.† The findings concluded that the fluorescent probe demonstrates a high degree of stability across these different conditions. The quantum yields of LYS@Au NCs and LYS@Ag/Au NCs were determined to be 3.96% and 9.45%, respectively. Table 1 presents a comparison of quantum yield values between Ag/Au NCs and others documented in literature. The as-prepared fluorescent probe demonstrates a favorable quantum yield as compared to the previously reported probes.

Table 1 Comparison between quantum yields of the as-fabricated Ag/Au NCs and other reported Ag/Au NCs

Fluorescent probe	Quantum yield (%)	Reference
Ag/Au NCs	3.00	37
	6.45	38
	7.30	39
	5.40	40
	9.0	41
	3.4	42
	6.4	43
	9.45	This work

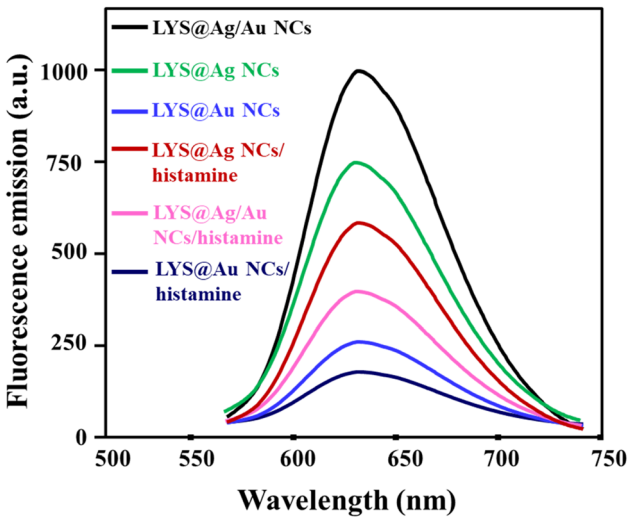

Fig. 3 The fluorescence responses of different probes in the presence and absence of histamine (350 μM).

3.2. Fluorescence responses of various probes

Fig. 3 illustrates the fluorescence responses of various probes in presence and absence of histamine. These probes comprised LYS@Ag NCs, LYS@Au NCs, and LYS@Ag/Au NCs. The addition of histamine (350 μM) to LYS@Ag NCs, LYS@Au NCs, and LYS@Ag/Au NCs resulted in relative fluorescence intensity changes of 21.0%, 15.4%, and 57.0%, respectively. This indicates that LYS@Ag/Au NCs exhibited significantly the higher fluorescence intensity change and a more pronounced reduction upon histamine addition compared to the other probes.

3.3. Reaction variables optimization

Fig. S4† illustrates the optimal conditions for the interaction between the fluorescent probe and histamine, including the incubation time and the diluting solvents. As depicted in Fig. S4A,† the optimum incubation time between the fluorescent probe and histamine is determined to be 3 minutes. Furthermore, the impact of various diluting solvents on the fluorescence response was investigated, as shown in Fig. S4B.† It was observed that water, with a pH of 7.0, yielded an identical response to buffer solutions. Hence, water was identified as the suitable medium for the interaction between histamine and LYS@Ag/Au NCs.

3.4. Detection of histamine using LYS@Ag/Au NCs

The fluorescent probe, once fabricated, was employed for the determination of histamine under optimal conditions. The results indicated that the fluorescence responses exhibited

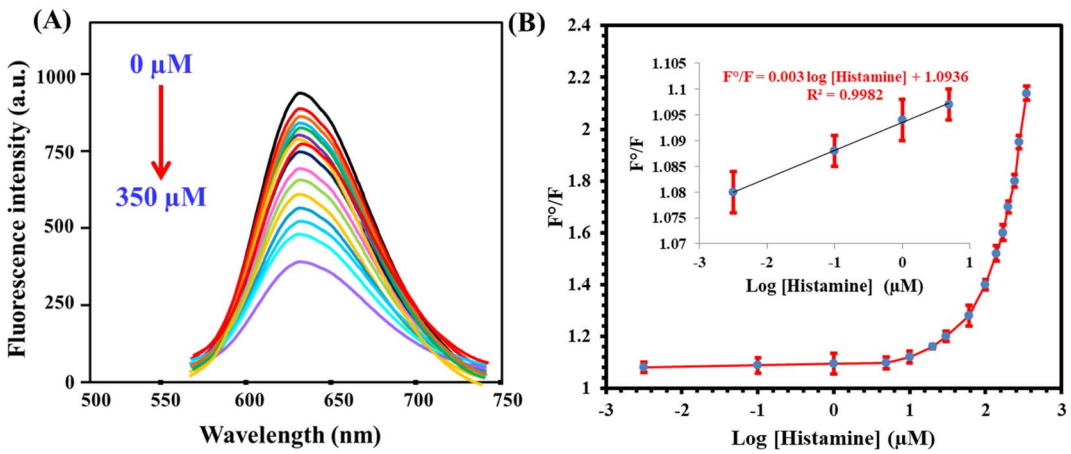

Fig. 4 (A) The influence of histamine addition (0.003–350 μM) on the fluorescence emission of the fluorescent probe. (B) Corresponding calibration plot.

Table 2 Comparison between analytical parameters of LYS@Ag/Au NCs and other fluorometric probes[a]

Probe	Linear range (μM)	LOD (μM)	Incubation time (min)	Reference
MOF-on-MOF	0.02–3.6	0.013	20	44
EDA-MQDs	1–60	0.046	10	45
DPA-CuNPs	0.05–5	0.003	10	46
Carbon nitride	5–800	2.34	15	47
BSA@AgAuNCs	0.01–80	0.003	3	48
o-Phthaldialdehyde/MIP	1.80–44.98	1.80	240	49
LYS@Ag/Au NCs	0.003–350	0.001	3	This work

[a] MOF: metal organic framework; EDA-MQDs: ethylene diamine-modified MXene quantum dots; DPA: D-penicillamine; CuNPs: copper nanoparticles; BSA: bovine serum albumin; MIP: molecularly-imprinted polymer.

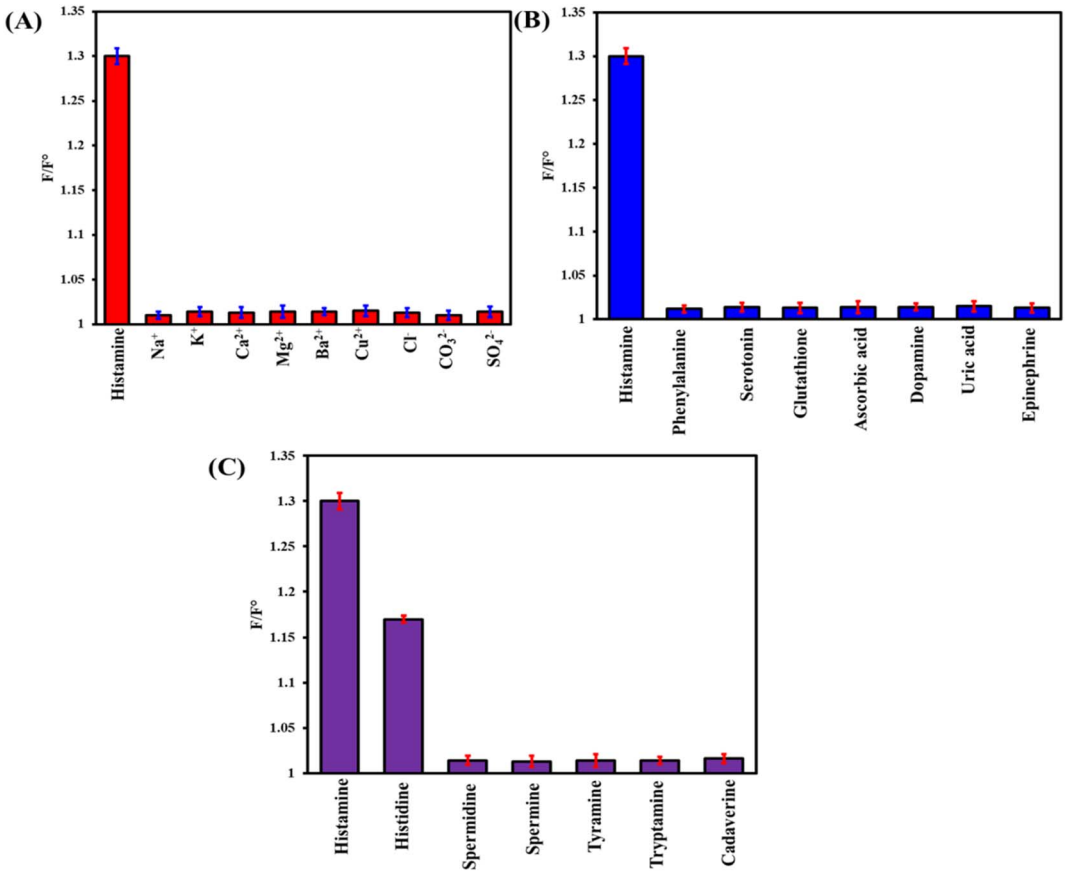

Fig. 5 The anti-interference capability of LYS@Ag/Au NCs towards histamine (60 μM) estimation in the presence of (A) 650 μM ions, (B) 350 μM biomolecules, and (C) 240 μM biogenic amines.

a direct relationship with the concentration of histamine within the range of 0.003 to 350 μM, as illustrated in Fig. 4A. The calibration plot, correlating the fluorescence ratio (F/F^0, where F and F^0 denote emission readings after and before histamine addition, respectively) to the histamine concentration, can be expressed by the equation: $F/F^0 = 1.09 + 0.003 \log[\text{histamine}]$ ($R^2 = 0.9987$) (Fig. 4B). The detection limit, determined based on a signal-to-noise ratio of 3 : 1, was found to be 0.001 μM. Furthermore, the analytical parameters of the developed sensor were compared with those of other reported sensors designed for histamine detection (Table 2). It was observed that the proposed probe offered several advantages, including a wide linear range and a low limit of detection (LOD) value.

3.5. Selectivity

The anti-interference ability of the as-prepared probe was assessed in the presence of 650 μM ions, 350 μM biomolecules, and 240 μM biogenic amines (Fig. 5). Only histamine can quench the fluorescence of LYS@Ag/Au NCs. However, due to the structural similarity between histamine and histidine, the fluorescent probe exhibited poor selectivity towards histamine in the presence of histidine. To mitigate this interference, histidine can be extracted using a Supelclean™ LC-SAX solid-phase extraction column. In this column, histidine can be removed by eluting with NH_4OH/CH_3COONH_4 (pH 10.0), while the neutral histamine (at this pH) strongly interacts with ($-NH_4^+$ in the column) and can be eluted using an acidic mobile phase.

3.6. Applications

The fluorescent probe was used to detect histamine in real samples. Fig. 6 displays the fluorescence spectra of LYS@Ag/Au NCs in human serum and canned tuna fish samples. The results obtained from the analysis of serum and tuna samples are summarized in Tables S1 and S2,† respectively. These findings substantiate the reliability of the proposed sensor for the accurate determination of histamine in complex matrices.

3.7. Detection mechanism

Investigating the sensing mechanism behind the quenching of LYS@Ag/Au NCs by histamine involved employing a range of techniques; including TEM, spectroscopy, DLS, fluorescence lifetimes, and zeta potentials (Fig. S5†). TEM scanning provided visualization of the average particle size of LYS@Ag/Au NCs both before and after histamine addition (Fig. S5A†). It was observed that the particle size increased significantly from 3.6 nm ± 0.21 nm to 120.46 nm ± 6.34 nm post histamine addition, indicating agglomeration. The quenching of LYS@Ag/Au NCs' fluorescence emission was attributed to an aggregation-

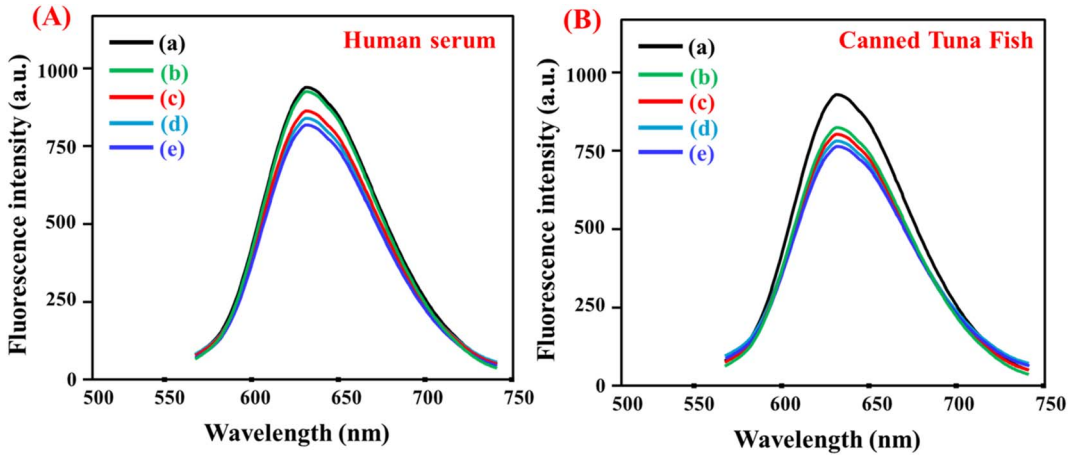

Fig. 6 Application of LYS@Ag/Au NCs fluorescent probe for detection of histamine in (A) human serum sample ((a) in water; (b) human serum; (c) 0.5 μM; (d) 3.0 μM; (e) 5.0 μM) and (B) canned tuna fish sample ((a) in water; (b) canned tuna fish extract; (c) 0.5 mg kg^{-1}; (d) 3.0 mg kg^{-1}; (e) 5.0 mg kg^{-1}).

enhanced quenching process.[50] Fig. S5B† demonstrated no overlap between the absorption spectrum of histamine and the fluorescence spectrum of LYS@Ag/Au NCs, ruling out a fluorescence resonance energy transfer (FRET) and inner filter effect (IFE). DLS analysis (Fig. S5C and D†) revealed hydrodynamic diameter shifts, indicating agglomeration post-histamine addition. The hydrodynamic diameters of LYS@Ag/Au NCs and LYS@Ag/Au NCs/histamine were determined as 86.5 nm ± 4.34 nm and 218.9 nm ± 8.28 nm, respectively. Fluorescence lifetimes measurement (Fig. S5E†) showed slight changes, with lifetimes of 4.56 ns for LYS@Ag/Au NCs and 4.59 ns for LYS@Ag/Au NCs/histamine, suggesting static quenching.[51] Zeta potential analysis (Fig. S5F†) depicted a decrease in charge, from −32.87 mV for LYS@Ag/Au NCs to −16.89 mV for LYS@Ag/Au NCs/histamine. This decrease indicated that positively charged histamine neutralized some of the negative charge on LYS@Ag/Au NCs, contributing to their destabilization and subsequent agglomeration.[52] In summary, the addition of histamine facilitated the aggregation of LYS@Ag/Au NCs through electrostatic interaction and hydrogen bond formation. This aggregation disrupted the fluorescence emission of LYS@Ag/Au NCs, resulting in fluorescence changes for the fluorescent probe.

4. Conclusion(s)

A novel "turn-off" fluorescent probe has been developed for the fluorescence sensing of histamine, employing gold nanoclusters doped with silver and stabilized by lysine amino acid (LYS@Ag/Au NCs). In the presence of histamine, the fluorescence emission of LYS@Ag/Au NCs decreased due to electrostatic interaction and hydrogen bond formation. The response ratio exhibits a direct linear relationship with the histamine concentration within the range of 0.003–350 μM. The limit of detection (LOD) is determined to be 0.001 μM based on a signal-to-noise ratio of 3 : 1. The fluorescent probe demonstrates a wide linear range, low detection limit, and good selectivity. Furthermore, the LYS@Ag/Au NCs probe has been successfully applied to detect histamine in various complicated samples, yielding acceptable results. This highlights the potential practical applicability of the probe in real-world scenarios.

Conflicts of interest

The authors declare no competing interests.

Acknowledgements

The authors are thankful to the Deanship of Graduate Studies and Scientific Research at Najran University for funding this work under the Growth Funding Program grant code (NU/GP/MRC/13/737-1).

References

1 H. J. Fu, R. F. Su, L. Luo, Z. J. Chen, T. J. Sorensen, N. Hildebrandt and Z. L. Xu, *ACS Sens.*, 2022, 7(4), 1113–1121.
2 A. M. Mahmoud, S. A. Alkahtani, B. A. Alyami and M. M. El-Wekil, *Anal. Chim. Acta*, 2020, **1133**, 58–65.
3 M. H. Mahnashi, A. M. Mahmoud, K. Alhazzani, A. Z. Alanazi, M. M. Algahtani, A. M. Alaseem, Y. S. A. Alqahtani and M. M. El-Wekil, *Microchem. J.*, 2021, **168**, 106439.
4 M. Moniente, D. García-Gonzalo, I. Ontañón, R. Pagán and L. Botello-Morte, *Compr. Rev. Food Sci. Food Saf.*, 2021, **20**, 1481–1523.
5 I. M. Sánchez-Guerrero, J. B. Vidal and A. I. Escuderom, *J. Allergy Clin. Immunol.*, 1997, **100**(3), 433–434.
6 S. L. Taylor and R. R. Eitenmiller, *Crit. Rev. Toxicol.*, 1986, **17**(2), 91–128.
7 D. A. Levy, Histamine and serotonin, *Mediators of Inflammation*, ed. G. Weissmann, Springer, US, Boston, 1974, pp. 141–159.

8 E. R. Lieber and S. L. Taylor, *J. Food Sci.*, 1977, **42**, 1584–1586.
9 M. P. V. Matos and S. Genualdi, *J. Food Compos. Anal.*, 2024, **127**, 105935.
10 X. Q. Lu, S. Y. Ji, Z. B. Ren, S. K. Jiang, Q. Yu, J. Q. Guo, A. X. Wang and X. M. Kong, *J. Chromatogr. A*, 2023, **1696**, 463953.
11 E. Kouti, A. Tsiasioti, C. K. Zacharis and P. D. Tzanavaras, *Microchem. J.*, 2021, **168**, 106513.
12 Y. F. Li, Z. Z. Lin, C. Y. Hong and Z. Y. Huang, *Food Chem.*, 2021, **345**, 128812.
13 A. M. Mahmoud, M. M. El-Wekil, M. H. Mahnashi, M. F. B. Ali and S. A. Alkahtani, *Microchim. Acta*, 2019, **186**, 617.
14 M. M. El-Wekil, A. M. Mahmoud, S. A. Alkahtani, A. A. Marzouk and R. Ali, *Biosens. Bioelectron.*, 2018, **109**, 164–170.
15 S. A. Alkahtani, A. M. Mahmoud, M. H. Mahnashi, R. Ali and M. M. El-Wekil, *Biosens. Bioelectron.*, 2020, **150**, 111849.
16 A. M. Mahmoud, S. S. Abu-Alruba, A. O. Al-Qarnia, M. M. El-Wekil and R. Y. Shahin, *Spectrochim. Acta, Part A*, 2024, **310**, 123850.
17 P. Li and H. R. Li, *Coord. Chem. Rev.*, 2021, **441**, 213988.
18 X. B. Lin, C. Y. Hong, Z. Z. Lin and Z. Y. Huang, *J. Food Compos. Anal.*, 2022, **112**, 104659.
19 F. Li, Z. Z. Lin, C. Y. Hong and Z. Y. Huang, *Food Chem.*, 2021, **345**, 128812.
20 H. H. Xie, L. Han and S. F. Tang, *Food Chem.*, 2024, **433**, 137314.
21 Y. R. Cao, X. C. Wang, T. Y. Feng, Z. J. Li, C. H. Xue and J. Xu, *Food Chem.*, 2022, **390**, 133194.
22 S. Li, G. Li, H. Shi, M. Yang, W. Tan, H. Wang and W. Yang, *Microchem. J.*, 2022, **175**, 107222–107229.
23 A. M. Mahmoud, M. H. Mahnashi and M. M. El-Wekil, *Spectrochim. Acta, Part A*, 2024, **304**, 123347.
24 B. A. Alyami, A. M. Mahmoud, A. O. Alqarni, A. B. H. Ali and M. El-Wekil, *Microchim. Acta*, 2023, **190**, 467.
25 J. Meng, X. Wei, X. Chen and J. Wang, *ACS Appl. Mater. Interfaces*, 2019, **11**(23), 21150–21158.
26 Z. Wang, Z. Zhu, C. Zhao, Q. Yao, X. Li, H. Liu, F. Du, X. Yuan and J. Xie, *Chem.–Asian J.*, 2019, **14**, 765–769.
27 P. R. Selvakannan, S. Mandal, S. Phadtare, R. Pasricha and M. Sastry, *Langmuir*, 2003, **19**, 3545–3549.
28 Y. Gao, C. Wang, C. Zhang, H. Li and Y. Wu, *Microchim. Acta*, 2021, **188**, 50.
29 M. Kumar and S. Deka, *ACS Appl. Mater. Interfaces*, 2014, **6**, 16071–16081.
30 X. F. Jia, X. Yang, J. Li, D. Y. Li and E. K. Wang, *Chem. Commun.*, 2014, **50**, 237–239.
31 S. A. Alkahtani, A. M. Mahmoud, R. M. K. Mohamed and M. M. El-Wekil, *Microchem. J.*, 2023, **195**, 109404.
32 A. M. Mahmoud, M. M. El-Wekil, R. Ali, H. A. Batakoushy and R. Y. Shahin, *Microchim. Acta*, 2022, **189**, 183.
33 A. O. Alqarni, S. A. Alkahtani, A. M. Mahmoud and M. M. El-Wekil, *Spectrochim. Acta, Part A*, 2021, **248**, 119180.
34 C. N. Iswarya, S. C. G. K. Daniel and M. Sivakumar, *Mater. Sci. Eng. C*, 2017, **75**, 393–401.
35 A. M. Mahmoud, S. S. Abu-Alrub, A. O. Al-Qarni, B. A. Alyami, M. M. El-Wekil and M. Oraby, *Microchem. J.*, 2024, **199**, 110012.
36 Y. Yang, Y. Sun, S. Liao, Z. Wu and R. Yu, *Anal. Methods*, 2016, **8**, 7237–7241.
37 M. Wang, X. Zhou, X. Wang, M. Wang and X. Su, *Sens. Actuators, B*, 2021, **345**, 130407.
38 J. Jana, P. Acharyya, Y. Negishi and T. Pal, *ACS Omega*, 2018, **3**, 3463–3470.
39 D. Ungor, I. Szilágyi and E. Csapó, *J. Mol. Liq.*, 2021, **338**, 116695.
40 L. Tian, Y. Li, T. Ren, Y. Tong, B. Yang and Y. Li, *Talanta*, 2017, **170**, 530–539.
41 Y. Zhang, H. Jiang, W. Ge, Q. Li and X. Wang, *Langmuir*, 2014, **30**, 10910–10917.
42 H. Sun, T. Qing, X. He, J. Shangguan, R. Jia, H. Bu, J. Huang and K. Wang, *Anal. Chim. Acta*, 2019, **1070**, 88–96.
43 H. Huang, H. Li, J. Feng and A. Wang, *Sens. Actuators, B*, 2016, **223**, 550–556.
44 Y. Yang, Z. Zhou, T. Wang, D. Tian, S. Ren and Z. Gao, *Talanta*, 2024, **270**, 125632.
45 T. Wang, W. Xiong, X. Tian and X. Xu, *Microchem. J.*, 2023, **194**, 109370.
46 X. Zhang, Q. Liu, Z. W. Wang, H. Xu, F. P. An, Q. Huang, H. B. Song and Y. W. Wang, *Microchim. Acta*, 2020, **187**, 329.
47 X. Lin, C. Hong, Z. Lin and Z. Huang, *J. Food Compos. Anal.*, 2022, **112**, 104659.
48 B. A. Alyami, A. M. Mahmoud, A. O Alqarni and M. M. El-Wekil, *Microchem. J.*, 2023, **195**, 109388.
49 X. Feng, J. Ashley, T. Zhou, A. Halder and Y. Sun, *RSC Adv.*, 2018, **8**, 2365–2372.
50 P. C. Wu, C. Y. Chen and C. W. Chang, *New J. Chem.*, 2018, **42**, 3459–3464.
51 U. Sivasankaran, S. Jesny, A. R. Jose and K. G. Kumar, *Anal. Sci.*, 2017, **33**, 281–285.
52 J. Bi, C. Tian, G. L. Zhang, H. Hao and H. M. Hou, *Foods*, 2020, **9**, 316.